Directed effective connectivity of cortical neuronal networks grown in vitro

Chumin Sun, K.C. Lin, C.Y. Yeung, and Emily S.C. Ching*
Institute of Theoretical Physics and Department of Physics, The Chinese University of Hong Kong, Shatin, Hong Kong

Yu-Ting Huang[1,2], Pik-Yin Lai[1], and C.K. Chan[2]
[1]*Dept. of Physics and Center for Complex Systems, National Central University, Chungli, Taiwan 320, ROC and*
[2]*Institute of Physics, Academia Sinica, Taipei, Taiwan 115, ROC*
(Dated: May 5, 2021)

In this paper, we apply a method that reconstructs directed networks from dynamics [Ching and Tam, Phys. Rev. E **95**, 010301(R), 2017] to reveal directed effective connectivity and synaptic weights of cortical neuronal cultures from multielectrode array recordings. The effective connectivity obtained reproduces several features of cortical regions in rats and monkeys and of the nematode C. elegans chemical synaptic network. The distribution of the incoming degree is bimodal and the distributions of the average incoming and outgoing synaptic strength are non-Gaussian with long tails. The effective connectivity captures different information from the functional connectivity that is estimated using statistical correlation between spiking activity. We show that spiking activity increases with the average synaptic strength of excitatory incoming and outgoing links in effective connectivity but not functional connectivity and thus demonstrate that effective connectivity can better reveal relationship between network structure and dynamics.

PACS numbers:

I. INTRODUCTION

The study of networks [1–3] has emerged in many branches of science. Many systems of interest consist of a large number of components that interact with each other and can be described as complex networks with the individual components being the nodes and the interactions among the nodes represented by links joining the nodes. Understanding the relationships between network structure, which depicts the linkage of nodes, and dynamics and function is a great challenge in neuroscience [4, 5] and in biology in general. Neuronal cultures grown in vitro serve as simple but yet useful experimental model systems for studying the relationship between network structure and the rich dynamics observed [6–8]. One common technique used to record the activity of neurons in a culture is the measurement of the electrophysiological signals generated by neurons using multielectrode array (MEA) [9]. Estimating network structure of neuronal cultures from MEA recordings is thus a problem of interest. Existing methods focus on estimating the functional connectivity, which is defined by statistical dependency between measurements [10], using statistical correlation [11–13] or mutual information [14, 15] of detected spikes in the MEA recordings. As statistical dependency can arise from indirect interactions, functional connectivity does not necessarily capture causal interactions. Causal interaction, referred to as effective connectivity [10], is more relevant for studying the relationships between network structure and dynamics and between network structure and function. Earlier studies of systems governed by a set of stochastic differential equations have shown that the covariance of nodal dynamics does not carry sufficient information to recover the effective connectivity [16, 17] of networks with directional coupling. For a general class of undirected networked systems with bidirectional coupling, it has been found that information of effective connectivity is contained in the inverse of the covariance matrix and not the covariance matrix itself [18–20]. This result can therefore explain the finding that a neural population can be strongly coupled but have weak pairwise correlation [21]. For systems with directional coupling, a noise-induced relation between the time-lagged covariance and the equal-time covariance of the dynamics has been found [22–25]. Using this covariance relation, a method that reconstructs the directed networks from dynamics has been proposed and validated using numerical simulations [17, 24, 26].

In this paper, we apply this covariance-relation based method to estimate the directed effective connectivity of in vitro cortical neuronal cultures of rat embryos from MEA recordings. In Sec. II B, we present details of the experimental measurements and discuss how we adopt the method with suitable modifications to obtain the directed effective connectivity matrix from the MEA recordings. In Sec. III, we present and discuss the results of the effective connectivity obtained. We compare the effective connectivity and functional connectivity based on statistical correlation of spiking activity estimated from the same sets of measurements in Sec. IV and show that effective connectivity can better reveal relationships between network structure and dynamics. Finally, we end the paper by a summary and conclusions in Sec. V.

*Corresponding author; email address: ching@phy.cuhk.edu.hk

II. DATA AND METHOD

A. Experimental measurements

Tissues were dissected from 2 to 3 rats and digested with 0.125 % trypsin for 15 min at 37°C. A small drop (100 μl) of cell suspension, containing about 6×10^4 cells, was plated on the 6 mm × 6 mm working area of the complementary metal-oxide-semiconductor (CMOS)-based high density multielectrode array (HD-MEA), which was pre-coated with 0.1 % Poly-D-lysine (Sigma P6407) and 0.1 % adhesion proteins laminin (Sigma L2020) (see Fig 1). After plating on the HD-MEA chip, cultures were filled with 1 ml of culture medium [DMEM (Gibco 10569) + 5% FBS (Gibco 26140) + 5% HS (Gibco 16050) + 1% PS (Gibco 15140)] and placed in a humidified incubator (5% CO_2, 37°C). Half of the medium was replaced by Neurobasal medium supplemented with B27 [Neurobasel medium (Gibco. 21103) + 2% 50X B27 supplement (Gibco. 17504) + 200 μM GlutaMAX (Gibco 35050)] twice a week.

The HD MEA probe (HD-MEA Arena, 3Brain AG) has 4096 electrodes arranged in a 64 by 64 square grid. The size of each square electrode is 21 μm by 21μm and the electrode pitch is 42 μm which gives an active electrode area of 2.67 mm by 2.67 mm. Neuronal activities from HD MEA were recorded with the recording device (BioCAM, 3Brain AG) and the associate software (BrainWave 2.0, 3Brain AG) at 7.06 kHz. One electrode was used for calibration purpose so there were 4095 electrodes that recorded signals. Spontaneous activities were recorded. Samples were placed into the recording device 10 min before the recording in order to prevent the effects of vibration. Each experimental session lasted for 5 min and was recorded in dark since the CMOS is a light active material.

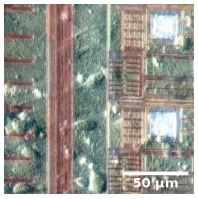

FIG. 1: Surface of high-density CMOS MEA. The line shows a scale of 50μm.

B. Method of reconstruction of effective connectivity

We treat the signal $x_i(t)$ recorded by each electrode as the activity of a node of the network as in [11]. We model the dynamics by a generic stochastic dynamical system

$$\frac{d\mathbf{x}}{dt} = \mathbf{F}(\mathbf{x}) + \eta \tag{1}$$

where $\mathbf{x} = (x_1, x_2, \ldots, x_N)$ with $N = 4095$ and η is a Gaussian white noise of zero mean and $\overline{\eta_i(t)\eta_j(t')} = D_{ij}\delta(t-t')$ and mimics external influences. The overbar denotes an ensemble average over different realization of the noise. We assume that the system has a fixed point $\mathbf{x}^*$ in the noise-free limit and linearize the equations around the fixed point to obtain

$$\frac{d\delta x_i}{dt} = \sum_j w_{ij}\delta x_j + \eta_i, \tag{2}$$

where $\delta x_i(t) = x_i(t) - x_i^*$ and $w_{ij} \equiv \partial F_i/\partial x_j(\mathbf{x}^*)$ are the elements of $\mathbf{W}$. When the activity x_j affects the activity x_i, w_{ij} is nonzero and represents the synaptic weight of the link from node j to node i, otherwise $w_{ij} = 0$ and there does not exist a link from node j to node i. Thus $\mathbf{W}$ is the directed and weighted effective connectivity matrix of the network which we would like to recover from the measurements of $x_i(t)$'s.

We define the elements of the time-lagged covariance matrix $\mathbf{K}(\tau)$ and the equal-time covariance matrix $\mathbf{K}(0)$ by

$$K_{ij}(\tau) = \langle [x_i(t+\tau) - \langle x_i(t+\tau)\rangle][x_j(t) - \langle x_j(t)\rangle]\rangle \tag{3}$$
$$K_{ij}(0) = \langle [x_i(t) - \langle x_i(t)\rangle][x_j(t) - \langle x_j(t)\rangle]\rangle. \tag{4}$$

where $\langle \ldots \rangle$ denotes a time average. Solving Eq. (2), it has been found that [16, 22–24]

$$\mathbf{K}(\tau) = \exp(\tau\mathbf{W})\mathbf{K}(0) \tag{5}$$

which implies

$$\mathbf{M} \equiv \frac{1}{\tau}\log(\mathbf{K}(\tau)\mathbf{K}(0)^{-1}) = \mathbf{W} \tag{6}$$

as long as τ is not too large [24]. Here, log is the principal matrix logarithm. The importance of Eq. (6) is that the off-diagonal elements M_{ij} of the matrix $\mathbf{M}$ are proportional to w_{ij} and thus should separate into two groups corresponding to $w_{ij} = 0$ (no links from node j to node j) and $w_{ij} \neq 0$ (links from node j to node i with weight w_{ij}). Hence we can infer w_{ij} by clustering M_{ij} into two groups. This covariance-relation based method to recover directed and weighted connectivity has been validated in numerical simulations of weighted directed random and scale-free networks with different nonlinear dynamics and coupling not only for the general class of systems as described above but also for some systems that do not approach a fixed point in the noise-free limit [24], including systems that obey the FitzHugh-Nagamo dynamics [27] with directional synaptic-like coupling that is commonly used to model neurons and other excitable systems [26].

The principal matrix logarithm is very sensitive to noise in measurements and a complex matrix could be resulted when the MEA recordings are directly used for the calculations. Let us denote the MEA recordings from the electrodes by $y_i(t)$, $i = 1, 2, \ldots, 4095$. We only analyze measurements taken during which all the 4095 electrodes

were recording properly. When we calculated $\mathbf{K}_y(\tau)$ and $\mathbf{K}_y(0)$ directly from $y_i(t)$ [as defined in Eqs. (3) and (4) with x_i replaced by y_i], we obtained a complex matrix $\log(\mathbf{K}_y(\tau)\mathbf{K}_y(0)^{-1})$. This problem has also been found in a study of effective connectivity of a cortical network of 68 regions from fMRI recordings and motivated the development of a Lyapunov optimization procedure [16]. Here, we avoid this problem by first applying a moving average filter to the MEA recordings. The moving average filter is a simple digital low-pass filter that is optimum for reducing random noise while retaining sharp transitions in the data [28]. Specifically, we take $x_i(t) = [y_i(t) + y_i(t + \Delta)]/2$, where $\Delta = 0.142$ ms is the sampling time interval and calculate $\mathbf{K}(\tau)$ and $\mathbf{K}(0)$ using $x_i(t)$ with $\tau = \Delta$. The resulting matrix $\mathbf{M}$ is now real. Then we extend the clustering analysis in Ref. [24] to estimate all the off-diagonal elements w_{ij}'s of the directed effective connectivity matrix as described below. By definition, $w_{ii} = 0$.

We assume that the outgoing links of each node, when exist, can only be all excitatory or all inhibitory. To infer the outgoing links of a certain node j, we fit the distribution of the values of M_{ij} for all $i \neq j$ by a Gaussian mixture model of two components, namely by a sum of two Gaussian distributions. This is done by using MATLAB 'fitgmdist', which returns the means, μ_1 and μ_2, and standard deviations, σ_1 and σ_2, of the two Gaussian components, and the relative proportion of the two components. Two examples are shown in Fig 2. When these two components are well separated with $|\mu_1 - \mu_2| > \sigma_1 + \sigma_2$, we identify the component of the larger proportion (greater than 0.6 of the whole distribution) as the unconnected component corresponding to $w_{ij} = 0$ assuming that the network is sparse. If none of the components has a relative proportion exceeding 0.6, we take the component whose mean is closer to zero as the unconnected component. The remaining component is referred as the connected component. If the connected component is on the right of the unconnected component as shown in the top panel of Fig 2, then node j is an excitatory node with all outgoing links of $w_{ij} > 0$. Otherwise if the connected component is on the left of the unconnected component as shown in the bottom panel of Fig. 2, then node j is an inhibitory node with all outgoing links of $w_{ij} < 0$. Next, we use MATLAB 'cluster' to obtain the posterior probability p_i of each of the M_{ij} values belonging to the unconnected component. If $p_i > 0.5$, then $w_{ij} = 0$ and there is no link from node j to node i. Otherwise if $p_i \leq 0.5$, then there is a link from node j to node i with a weight $w_{ij} = M_{ij} - \langle M_{kj} | w_{kj} = 0 \rangle_k$ where $\langle M_{kj} | w_{kj} = 0 \rangle_k$ is the average over k of those M_{kj} values that are estimated to correspond to $w_{kj} = 0$. We repeat this procedure for all the nodes j to estimate all the elements w_{ij}.

In the event that the two Gaussian components are not well separated but close to one another with $|\mu_1 - \mu_2| < \max(\sigma_1, \sigma_2)$, we fit the distribution of M_{ij} again by one single Gaussian distribution, denoted by P_G of mean μ,

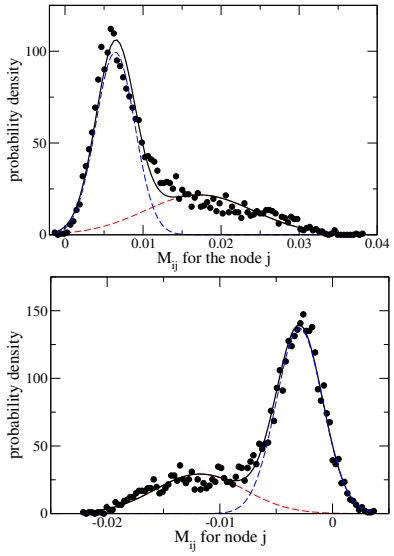

FIG. 2: The probability density of M_{ij} for node j (circles). The solid black line is the fit by a Gaussian mixture model of two components (two-Gaussian fit). The component with a larger relative proportion (blue dashed line) is identified as the unconnected component and the other component (red dashed line) is identified as the connected component. In the top panel, the connected component lies on the right of the unconnected component and the node j is inferred as an excitatory node. In the bottom panel, the connected component lies on the left of the unconnected component and the node j is inferred as an inhibitory node.

and identify the outliers, which are data points deviating significantly from P_G, with $w_{ij} \neq 0$. For this purpose, we let x_E and x_I be

$$x_E = \min_{x>\mu}\{P_K(x) = 3P_G(x)\} \tag{7}$$

$$x_I = \max_{x<\mu}\{P_K(x) = 3P_G(x)\} \tag{8}$$

where P_K is the distribution of M_{ij} obtained by the Kernel density estimation and calculate the number of data points, denoted by N_1, that satisfy $M_{ij} > x_E$ and the number of data points, denoted by N_2, that satisfy $M_{ij} < x_I$. If $N_1 > N_2$, then the N_1 data points satisfying $M_{ij} > x_E$ are the outliers otherwise if $N_2 > N_1$, then the N_2 data points satisfying $M_{ij} < x_I$. The identified outliers are then inferred to have $w_{ij} = M_{ij} - \langle M_{kj} | w_{kj} = 0 \rangle_k$. If both $N_1 = N_2 = 0$, then node j is inferred to have no detectable outgoing links. For the in-between cases of the two Gaussian components that are neither well separated nor too close to each other with $\max(\sigma_1, \sigma_2) \leq |\mu_1 - \mu_2| \leq \sigma_1 + \sigma_2$, we choose either the two-Gaussian fit or the single-Gaussian fit according to the Bayesian information criterion for fitting models selection [29, 30].

III. RESULTS OF THE EFFECTIVE CONNECTIVITY

We estimate the directed effective connectivity for 8 cases using MEA recordings taken at 8 different Days in Vitro (DIV) and study the basic network measures and the distributions of degree and synaptic strength.

A. Basic network measures

We calculate several basic network measures including the connection probability p, the ratio r_B of the number of bidirectionally connected pairs to the expected number for a random network with same connection probability p, the fractions f_E and f_I of excitatory and inhibitory nodes, the fraction $f_{\rm SCC}$ of nodes that form the strongly connected component, the characteristic path length l, the average clustering coefficient (CC) and the small world index (SWI). The results are shown in Table I. The connection probability p of a network of N nodes with N_L links is defined by $p = N_L/[N(N-1)]$. We find that p ranges from 0.7-1.9% which is consistent with our assumption that the neuronal networks are sparse. This average value of p is smaller but comparable to that of the chemical synapse network of C. elegans [31]. Most of the connections are unidirectional in accord with the directional transmission of signals in neurons. One expects neuronal networks to be organized and thus highly nonrandom in order to facilitate effective and efficient signal transmission. For a random network of n nodes and connection probability p, the expected number of bidirectionally connected pairs is given by $N(N-1)p^2/2$. We denote the ratio of the number of bidirectionally connected pairs in the network to the expected number in a random network by r_B. The values of r_B exceed 4 for all the networks, consistent with the well-documented overrepresentation of bidirectional connected pairs in local cortical circuits [32–35].

Each node is inferred as excitatory or inhibitory according to the sign of the synaptic weights of its outgoing links as discussed in Sec. II B. There is a small fraction of nodes with no detectable outgoing links. As can be seen in Table I, the values of f_I range from 0.13 to 0.31, which are comparable to the measured fractions (0.15-0.30) of inhibitory neurons in various cortical regions in monkey [36]. The balance between excitation and inhibition in the cortex is believed to play an important role in executing proper brain functions and disruption of such a balance may underlie the behavioral deficits that are observed in conditions such as autism and schizophrenia [37–41]. The fraction $f_{\rm SCC}$ of nodes that form the largest strongly connected component exceeds 70% for all the cases studied. The characteristic path length l, which is the average shortest path length for all nodes that can be connected by a finite path is about 4, and the average local clustering coefficient CC, which is the average of the connection probability of the outgoing neighbors of each node, ranges from $0.18 - 0.38$. These values are comparable to those of the chemical synapse network of C. elegans. Furthermore, the reconstructed neuronal networks all have small-world topology, with small-world index SWI substantially greater than one. It has been shown that small-world network allows efficient transmission of information [42].

B. Distributions of incoming and outgoing degrees

The distributions of the incoming and outgoing degrees are qualitatively the same for all the 8 cases and results for one case are shown in Fig. 3. There are several notable features. First, most of the nodes have a small $k_{\rm out}$ that is less than a few tens but a small fraction of nodes have an exceptionally large $k_{\rm out}$ exceeding a thousand. This is the case for both the excitatory and inhibitory nodes. Second, the incoming degree distribution is approximately bimodal, which is different from the approximate scale-free distribution found in functional connectivity [13] (see also Sec. IV). The bimodal feature of the incoming degree distribution is more clearly revealed in the separate distributions of the excitatory and inhibitory incoming degrees $k_{\rm in}^+$ and $k_{\rm in}^-$ for incoming links of positive and negative synaptic w_{ij}, respectively (see Fig. 4). By studying the distribution of $k_{\rm in}^+$ (or $k_{\rm in}^-$) separately for the two modes of nodes of small and large $k_{\rm in}^-$ ($k_{\rm in}^+$) (see inset of Fig. 4), it can be seen that nodes tend not to have both large $k_{\rm in}^+$ and large $k_{\rm in}^-$.

C. Distributions of average synaptic strength

Both in vitro and in vivo studies have indicated that the distribution of synaptic weights in the cortex are generally skewed with long tails and typically lognormal [43]. Motivated by these findings, we study the distributions of the average synaptic strength of the links. The various averages of the synaptic weights are defined as follows

$$s_{\rm in}(i) = \sum_j \frac{w_{ij}}{k_{in}(i)} \tag{9}$$

$$s_{\rm in}^+(i) = \frac{\sum_{j,w_{ij}>0} w_{ij}}{k_{\rm in}^+(i)} \tag{10}$$

$$s_{\rm in}^-(i) = \frac{\sum_{j,w_{ij}<0} w_{ij}}{k_{\rm in}^-(i)} \tag{11}$$

$$s_{\rm out}(i) = \frac{\sum_j w_{ji}}{k_{\rm out}(i)}. \tag{12}$$

Among these quantities, $s_{\rm in}^+ > 0$ is the average of the synaptic weights of excitatory incoming links and $s_{\rm in}^- < 0$ is the average of the synaptic weights of inhibitory incoming links, $s_{\rm in}$ is the average of the synaptic weights of all incoming links and can be positive or negative, and $s_{\rm out}$ is the average of the synaptic weights of all outgoing

	case 1	case 2	case 3	case 4	case 5	case 6	case 7	case 8	C. elegans
DIV	11	22	25	33	45	52	59	66	—
p (%)	1.2	1.9	1.4	1.5	1.1	1.7	1.4	1.5	2.8
r_B	5.9	5.5	10.7	5.7	6.5	4.21	4.0	4.4	—
f_E	0.62	0.80	0.84	0.75	0.62	0.66	0.48	0.57	—
f_I	0.27	0.13	0.14	0.18	0.21	0.24	0.32	0.28	—
$f_{\rm SCC}$	0.88	0.93	0.98	0.92	0.81	0.90	0.77	0.83	0.85
l	4.0	3.7	3.7	3.9	4.1	3.7	3.8	3.8	3.5
CC	0.26	0.36	0.38	0.30	0.25	0.28	0.18	0.22	0.22
SWI	13.1	11.3	17.1	12.7	14.4	10.4	7.9	8.8	2.3

TABLE I: Basic network measures of the networks reconstructed. When available, the corresponding results for the chemical synapse network of C. elegans [31] are included for comparison.

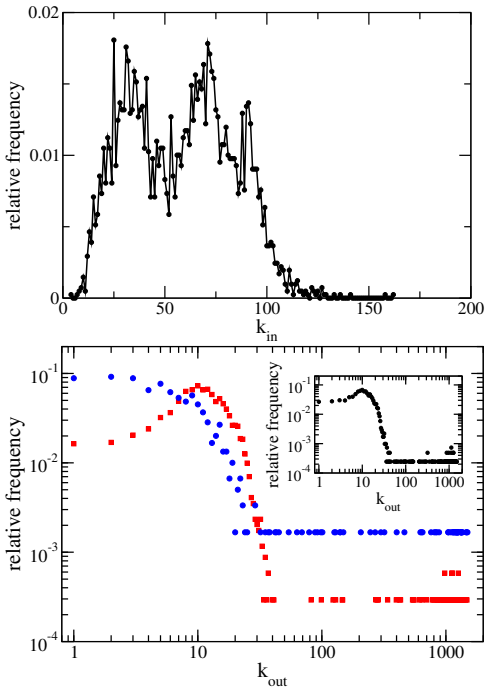

FIG. 3: Distributions of the incoming degree $k_{\rm in}$ (top panel) and outgoing degree $k_{\rm out}$ (bottom panel) of case 3. In the bottom panel, we show the distribution of $k_{\rm out}$ separately for excitatory (circles) and inhibitory nodes (squares) and for all the nodes in the inset.

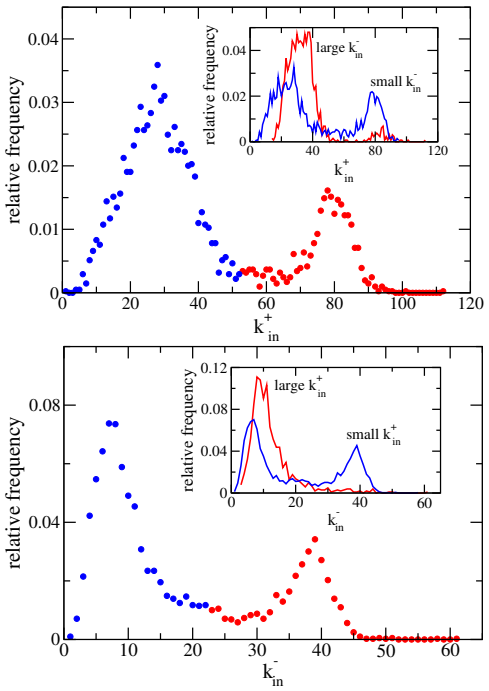

FIG. 4: Distributions of the excitatory and inhibitory incoming degrees, $k_{\rm in}^+$ (top panel) and $k_{\rm in}^-$ (bottom panel), of case 3. The distributions are clearly bimodal with two modes of large and small $k_{\rm in}^+$ or $k_{\rm in}^-$. In the insets, we show the relative frequencies separately for the two modes of nodes of small and large $k_{\rm in}^-$ (or $k_{\rm in}^+$).

links and is positive for excitatory nodes, negative for inhibitory nodes and zero for the nodes with no detectable outgoing links. To have better statistics, we use the data from all the 8 networks to calculate the distributions. We first calculate the mean and standard deviation of these average synaptic weights in each of the networks and then calculate the distribution of the standardized values, which are the values subtracted by the mean and divided by the standard deviation. The distribution of $s_{\rm out}$ for excitatory nodes is found to depend on whether $s_{\rm in}$ is positive or negative. As seen in Fig 5, all these average synaptic strengths have a non-Gaussian distribution that is skewed with long tails. This indicates that a small fraction of the nodes have dominantly strong average synaptic strengths and thus the average synaptic strength of the links of the nodes are not well represented by the mean values. We also calculate the distribution of the standardized values of the logarithm of these average synaptic strengths and find that $s_{\rm out}$ for excitatory nodes with $s_{\rm in} > 0$ has an approximately lognormal distribution (see Fig. 5).

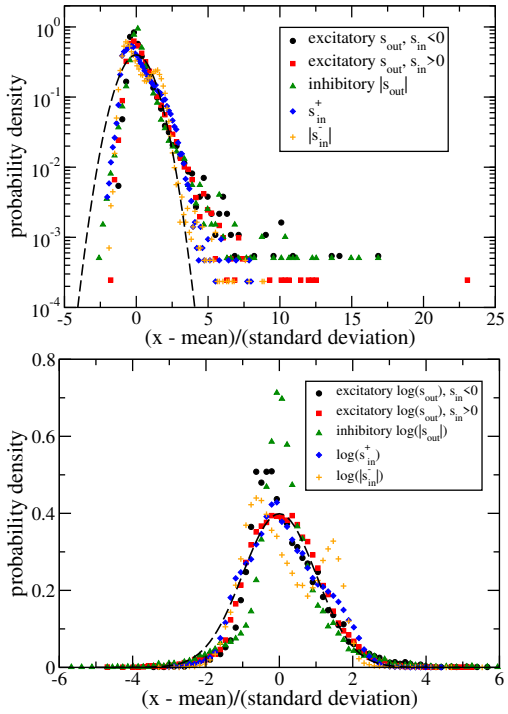

FIG. 5: Distributions of the average synaptic strengths of excitatory and inhibitory incoming links $s_{\rm in}^{+}$ and $s_{\rm in}^{-}$ and of outgoing links $s_{\rm out}$. Top panel: Distributions of the standardized values of the average synaptic strength, $(x - \text{mean})/(\text{standard deviation})$, where x is $s_{\rm in}^{+}$, $s_{\rm in}^{-}$ or $s_{\rm out}$ in each case. Bottom panel: Distributions of the standardized values of the logarithm of the average synaptic weights with x now being $\log(s_{\rm in}^{+})$, $\log(|s_{\rm in}^{-}|)$ or $\log(|s_{\rm out}|)$. The dashed line is the standardized Gaussian distribution.

D. Possible effects of hidden nodes

Neural cells lying in the working area outside the active electrode area of the MEA probe could form synaptic connections with cells within the active electrode area but their spontaneous activities were not recorded. Thus the MEA recordings could miss out information from those nodes that were not detected. These nodes are thus the so-called hidden nodes. It has been show that in bidirectional networks the presence of hidden nodes that are randomly missed out has no significant adverse effects on the reconstruction of the links among the measured nodes [44]. To investigate whether and how undetected signals from the hidden nodes might affect our results, we reconstruct a partial network using only recordings of 2025 electrodes, which are the 45 by 45 electrodes in the central region of the active electrode area, and compare it with the subnetwork of these corresponding 2025 nodes, extracted from the whole network that we reconstructed using recordings of all the 4095 electrodes for case 3. We find that the partial network captures correctly 99.8% of the non-existent links and 83.0% of the links in the subnetwork. Moreover, the partial network and the subnetwork have similar in- and out-degree distributions as shown in Fig. 6. These results support that the directed effective connectivity obtained using the 4095 electrodes is not significantly affected by the possible missed out signals from the neural cells lying outside the active electrode area of the MEA probe.

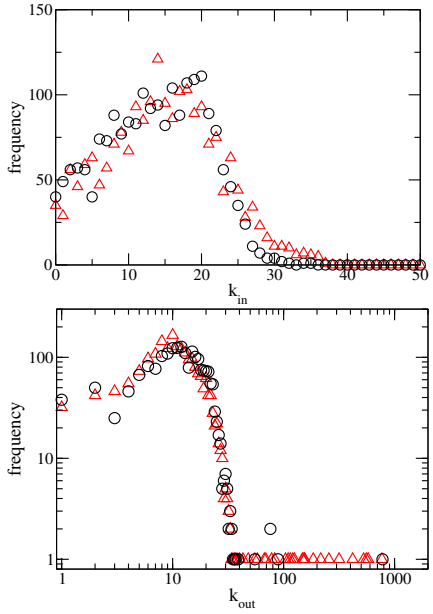

FIG. 6: Distributions of in- and out-degrees of the subnetwork (circles) and partial network (triangles) for case 3.

IV. COMPARISON OF EFFECTIVE CONNECTIVITY AND FUNCTIONAL CONNECTIVITY

The effective connectivity studied in the present work is proposed to capture causal relationships between the dynamics of the nodes based on the general class of model described in Eq. (1) while functional connectivity studied in existing methods is based mainly on the statistical dependence of the dynamics of the nodes. It is thus expected that effective connectivity and functional connectivity to contain different information about the system. In this Section, we compare directly the two types of connectivity estimated from the same sets of measurements. We follow the method in Ref. [13] to estimate the functional connectivity using the statistical correlation of the spikes detected from the MEA recordings. By applying the spike detection algorithm in the BrainWave software to the recorded time series $y_i(t)$ of the i-th electrode, we obtain the times of the spikes t_k^i, $k = 1, 2, \ldots, N_i$, for the N_i spikes detected for node i. The spike train $S_i(t)$ is constructed as follows: $S_i(t) = 1$ for $t = t_k^{(i)}$, $k = 1, 2, \ldots, N_i$ and 0 otherwise. The general idea is to estimate a functional link between nodes i and j when the correlation between the two spike trains exceeds a certain threshold. The cross-correlation of the spiking activity of nodes i

and j is measured by $C_{ij} \in [0,1]$, which is defined by [11]

$$C_{ij}(\tau) = \frac{1}{\sqrt{N_i N_j}} \langle S_i(t) S_j(t+\tau) \rangle \qquad (13)$$

In the earlier method [11], $C_{ij}(\tau)$ is calculated in a window of τ-values: $-n\Delta \leq \tau \leq n\Delta$, where Δ is the sampling time interval and if the maximum value $C_{ij}(\tau_0)$ at τ_0 within this window exceeds a certain threshold then a link of weight $C_{ij}(\tau_0)$ is inferred between nodes i and j j with the direction of the link determined by the sign of τ_0. To detect also inhibitory links with negative weights, $f_{ij}(\tau)$ measuring the difference of $C_{ij}(\tau)$ from its average value in the window has been introduced [13]

$$f_{ij}(\tau) = C_{ij}(\tau) - \frac{1}{2n+1} \sum_{k=-n}^{n} C_{ij}(k\Delta), \qquad (14)$$

which can assume both positive and negative values. In our calculations, we use $n = 100$. Let $|f_{ij}(\tau)|$ attains its maximum at $\tau = \tau^*$ [45]; a link is inferred for the functional connectivity, from node i to node j if $\tau^* > 0$ and from node j to node i if $\tau^* < 0$, with strength $f_{ij}(\tau^*)$ when $|f_{ij}(\tau^*)|$ exceeds a certain threshold and $|\tau^*|$ is not shorter than the time needed for a synaptic signal with a propagation speed of 400mm/s [13]. Excitatory links have $f_{ij}(\tau^*) > 0$ while inhibitory links have $f_{ij}(\tau^*) < 0$. The requirement that a node is either excitatory or inhibitory, with outgoing links having only one sign, cannot be enforced in this cross-correlation based method for estimating functional connectivity. This method also has a considerably weaker sensitivity for detecting inhibitory links [13]. In contrast, the covariance-relation based method that we use to estimate effective connectivity can detect excitatory and inhibitory links equally well using only a recording time of 5 min.

There is a relatively large fraction of nodes having zero incoming or outgoing degrees in the estimated functional connectivity. In Fig. 7, we show the distributions of nonzero incoming and outgoing degrees for functional connectivity. It can be seen that the two distributions are similar and are approximately scale-free with possibly different exponents for small and large degrees. This result is consistent with the scale-free degree distributions reported [13] but is clearly different from the bimodal incoming-degree distribution found in effective connectivity as shown in Fig. 3. We compare the strongest excitatory and inhibitory links estimated in the two types of connectivity in Fig. 8. We choose 200 excitatory links and 50 inhibitory links in the effective connectivity. It is not possible to choose exactly the same number of links in functional connectivity as many links have the same coupling strength and we choose the closest number of links for the comparison. In the effective connectivity, most of the strongest excitatory links are connecting nearby nodes. This feature is not found in the functional connectivity.

To check whether the proposed effective connectivity can indeed reveal relationships between network structure and dynamics better than functional connectivity, we study the relation between the spiking activity and the average synaptic strength of the nodes. Specifically, we divide the nodes into 15 groups according to their number of detected spikes and calculate the mean values of the average synaptic strength of excitatory and inhibitory incoming and outgoing links of these 15 groups. Since nodes have both excitatory and inhibitory outgoing links in functional connectivity, we generalize the definition of $s_{\rm out}$ to $s^+_{\rm out}$ and $s^-_{\rm out}$:

$$s^+_{\rm out}(i) = \frac{\sum_{j,w_{ji}>0} w_{ji}}{k^+_{\rm out}(i)} \qquad (15)$$

$$s^-_{\rm out}(i) = \frac{\sum_{j,w_{ji}<0} w_{ji}}{k^-_{\rm out}(i)}. \qquad (16)$$

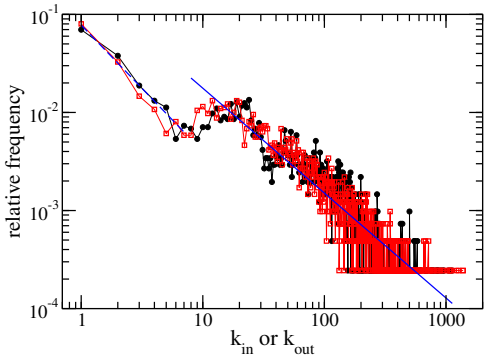

FIG. 7: Distributions of the incoming and outgoing degree, $k_{\rm in}$ (circles) and $k_{\rm out}$ (squares) of the functional connectivity estimated for case 3. The dashed and solid lines are power-law fits of the small- and large-degree regions of the distribution of $k_{\rm in}$.

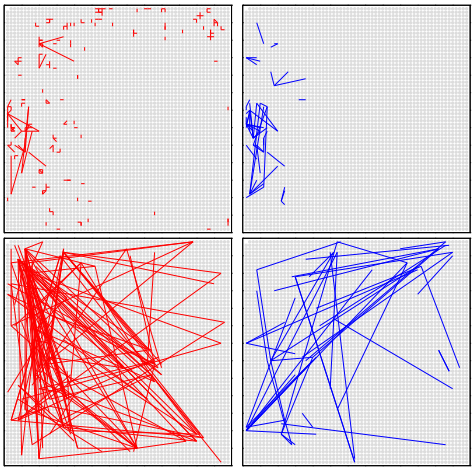

FIG. 8: Comparison of the strongest N_e excitatory (red) and the strongest N_i inhibitory links (blue) of the effective connectivity (top panels) and of the functional connectivity (bottom panels) for case 3. $N_i = 50$ for both types of connectivity, $N_e = 200$ for effective connectivity and $N_e = 151$ for functional connectivity.

For the effective connectivity, $s^+_{\rm out}$ ($s^-_{\rm out}$) is equal to $s_{\rm out}$ for excitatory (inhibitory) nodes. The results for the two types of connectivity are shown in Fig. 9. The dependence of spiking activity on $s^-_{\rm in}$ and $s^-_{\rm out}$ is weak for both types of connectivity. Definite relations between the spike rate and $s^+_{\rm in}$ and $s^+_{\rm out}$ are found in the effective connectivity but not in the functional connectivity. In particular, the intuition that nodes with larger $s^+_{\rm in}$ would spike more is confirmed in the effective connectivity but not functional connectivity. The effective connectivity further reveals that nodes that spike more have larger $s^+_{\rm out}$ on average and such a dependence is again lacking in the functional connectivity.

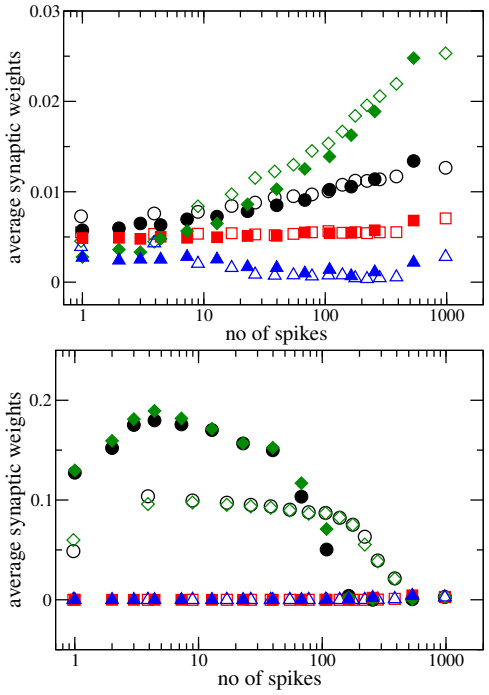

FIG. 9: The dependence of the mean values of $s^+_{\rm in}$ (circles), $s^-_{\rm in}$ (squares), $s^+_{\rm out}$ (diamonds) and $s^-_{\rm out}$ (triangles) on the number of detected spikes of the nodes in effective connectivity (top panel) and functional connectivity (bottom panel). The open symbols are for case 3 and the filled symbols are for case 5.

V. SUMMARY AND CONCLUSIONS

Revealing directed connectivity of neuronal networks from recordings taken by large-scale MEA is a challenging inverse problem. Existing methods focus on functional connectivity that is based on the statistical correlation of the detected spiking activities. However, to study relations between network structure and dynamics and network structure and functions of neuronal networks, effective connectivity which measures direct causal interactions is more relevant. In this paper, we have adopted a general method that reconstructs connectivity from dynamics [24] to estimate effective connectivity of neuronal cultures from MEA recordings. This method involves a calculation of a principal matrix logarithm, which is very sensitive to noise in the data. If the method is applied directly to the MEA recordings, a complex matrix would be obtained. By first applying a moving average filter to the MEA recordings to reduce the effect of noise, the problem of complex matrix has been avoided and we have successfully estimated the directed and weighted effective connectivity matrix of neuronal networks from recordings taken by MEA of over 4000 electrodes.

Our results of the effective connectivity reproduce various reported features of cortical regions in rats and monkeys and of the nematode C. elegans chemical synaptic network. The distributions of incoming and outgoing degrees are different from approximately scale-free distributions found in the functional connectivity. In particular the excitatory and inhibitory incoming degree distributions are found to be bimodal. There have been studies indicating that the robustness of undirected networks against both random failures and targeted attacks can be optimized by having a bimodal degree distribution [46, 47] and future studies are required to establish the significance of the bimodal feature of incoming degree distributions. We have found that the distributions of average synaptic strengths are non-Gaussian and skewed with a long tail and that the distribution of the average synaptic strength of outgoing links for excitatory nodes with positive average synaptic strength of incoming links ($s_{\rm in} > 0$) is approximately lognormal, and our results are consistent with reported results found in in vitro and in vivo studies of synaptic strengths in the cortex [43]. The significance of such non-Gaussian distributions with long tails is that a small fraction of nodes have dominantly strong average synaptic strength suggesting the possibility that the bulk of the information flow occurring mostly through them [43]. Understanding how the long-tailed synaptic strength distribution might be related to the spiking dynamics or the relations between network structure and dynamics in general will be a topic of interest in future studies.

The effective connectivity and functional connectivity estimated from the same sets of MEA recordings are different. We have shown that the spiking activity increases with the average synaptic strength of excitatory incoming and outgoing links in effective connectivity but not functional connectivity. These findings demonstrate that the effective connectivity proposed in the present work can indeed better reveal relationships between network structure and dynamics for neuronal cultures.

Acknowledgments

The work of CS, KCL, CYY and ESCC has been supported by the Hong Kong Research Grants Council under grants no. CUHK 14300914 and CUHK 14304017. PYL was supported by the Ministry of Science and Technology of the Republic of China under grant no. 107-2112-M-

008-013-MY3 and NCTS of Taiwan.

[1] S.H. Strogatz, Exploring complex networks, Nature (London) **410**, 268 (2001).

[2] R. Albert and A.-L. Barabási, Statistical mechanics of complex networks, Rev. Mod. Phys. **74**, 48 (2002).

[3] M.E.J. Newman, The Structure and Function of Complex Networks, SIAM Rev. **45**, 167 (2003).

[4] E. Bullmore and O. Sporns, Complex brain networks: graph theoretical analysis of structural and functional systems, Nat. Rev. Neurosci. **10**, 186 (2009)

[5] D.S. Bassett and O. Sporns, Network neuroscience, Nat. Neurosci. **20**, 353 (2017).

[6] J.P. Eckmann, O. Feinerman, L. Gruendinger, E. Moses, J. Soriano and T. Tlusty, The physics of living neural networks, Phys. Rep. **449**, 54 (2007).

[7] O. Feinerman, A. Rotem and E. Moses, Reliable neuronal logic devices from patterned hippocampal cultures, Nat. Phys. **4**, 967 (2008).

[8] J. Soriano, J. Casademunt, Neuronal cultures: The brain's complexity and non-equilibrium physics, all in a dish, Contrib. Sci. **11**, 225 (2015).

[9] M.E.J. Obien, K. Deligkaris, T. Bullmann, D.J. Bakkum and U. Frey, Revealing neuronal function through microelectrode array recordings, Front. Neurosci. **8**, 423 (2015).

[10] K.J. Friston, Functional and Effective Connectivity: A Review, Brain Connectivity **1**, 13-36 (2011).

[11] A. Maccoine, N. Garofalo, T. Nieus, M. Tedesco, L. Berdondini and S. Martinoia, Multiscale functional connectivity estimation on low-density neuronal cultures recorded by high-density CMOS Micro Electrode Arrays, J. NeuroSci. Methods **207**, 161-171 (2012).

[12] D. Poli, V.P. Pastore, and P. Massobrio, Functional connectivity in in vitro neuronal assemblies, Front. Neural Circuits **9**, 57 (2015).

[13] V.P. Pastore, P. Massobrio, A. Godjoski, S. Martinoia, Identification of excitatory-inhibitory links and network topology in large-scale neuronal assemblies from multi-electrode recordings, PLoS Comput. Biol. **14**, e1006381 (2018).

[14] L.M.A. Bettencourt, G.J. Stephens, M.I. Ham and G.W. Gross, Functional structure of cortical neuronal networks grown in vitro, Phys. Rev. E **75**, 021915 (2007).

[15] L.M.A. Bettencourt, V. Gintautas and M.I. Ham, Identification of Functional Information Subgraphs in Complex Networks, Phys. Rev. Lett. **100**, 238701 (2008).

[16] M. Gilson, R. Moreno-Bote, A. Ponce-Alvarez, P. Ritter and G. Deco, Estimation of Directed Effective Connectivity from fMRI Functional Connectivity Hints at Asymmetries of Cortical Connectome, PLoS Comput. Biol. **12**, e1004762 (2016).

[17] H.C. Tam, E.S.C. Ching and P.Y. Lai, Reconstructed networks from dynamics with correlated noise, Physica A **502**, 106-122 (2018).

[18] J. Ren, W.-X. Wang, B. Li, and Y.-C. Lai, Noise Bridges Dynamical Correlation and Topology in Coupled Oscillator Networks, Phys. Rev. Lett. **104**, 058701 (2010).

[19] E.S.C. Ching, P.Y. Lai and C.Y. Leung, Extracting connectivity from dynamics of networks with uniform bidirectional coupling, Phys. Rev. E **88**, 042817 (2013); Erratum, Phys. Rev. E **89**, 029901(E) (2014).

[20] E.S.C. Ching, P.Y. Lai and C.Y. Leung, Reconstructing Weighted Networks from Dynamics, Phys. Rev. E **91**, 030801(R) (2015).

[21] E. Schneidman, M.J. Berry, R. Segev and W. Bialek, Weak pairwise correlations imply strongly correlated network states in a neural population, Nature **440**, 1007 (2006).

[22] R.J. Prill, R. Vogel, G.A. Cecchi, G. Altan-Bonnet and G. Stolovitzky, Noise-Driven Causal Inference in Biomolecular Networks, PLoS ONE **10**, e0125777 (2015).

[23] B.J.Lüsmann, Reconstruction of Physical Interactions in Stationary Stochastic Network Dynamics, Master Thesis, Max Planck Inst. for Dynamics and Self-Organization (2015).

[24] E.S.C. Ching and H.C. Tam, Reconstructing links in directed networks from noisy dynamics, Phys. Rev. E **95**, 010301(R) (2017).

[25] P.Y. Lai, Reconstructing Network topology and coupling strengths in Directed Networks of discrete-time dynamics, Phys. Rev. E **95**, 022311 (2017).

[26] H.C. Tam, Reconstruction of Networks from Noisy Dynamics, Ph.D Thesis, The Chinese University of Hong Kong (2017).

[27] R. FitzHugh, Impulses and physiological states in theoretical models of nerve membrane, Biophys. J. **1**, 445 (1961).

[28] S.W. Smith, The Scientist and Engineer's Guide to Digital Signal Processing. 2nd ed. San Diego: California Technical Publishing; 1999.

[29] R.E. Kass, A.E. Raftery, Bayes factors, J. Amer. Stat. Assoc. **90**, 773-795 (1995).

[30] A.E. Raftery, Bayes factors and BIC: Comment on a critique of the Bayesian information criterion for model selection, Sociol. Methods Res. **27**, 411-427 (1999).

[31] L.R. Varshney, B.L. Chen, E. Paniagua, D.H. Hall and R.B. Chklovskii, Structural Properties of the Caenorhabditis elegans Neuronal Network, PLoS Comput. Biol. **7**, e1001066 (2011).

[32] S. Song, P.J. Sjöström, M. Reigl, S. Nelson and R.B. Chklovskii, Highly Nonrandom Features of Synaptic Connectivity in Local Cortical Circuits, PLoS Biology **3**, e350 (2005).

[33] H. Markram, J. Lübke, M. Frotscher, A. Roth and B. Sakmann, Physiology and anatomy of synaptic connections between thick tufted pyramidal neurones in the developing rat neocortex, J. Physio. **500**, 409-440 (1997).

[34] P.J. Sjöström, G.G. Turrigiano and S.B. Nelson, Rate, timing, and cooperativity jointly determine cortical synaptic plasticity, Neuron **32**, 1149-1164 (2001).

[35] R. Perin, T.K. Berger and H. Markram, A synaptic organizing principle for cortical neuronal groups, PNAS **108**, 5419-5425 (2001).

[36] S.H. Hendry, H.D. Schwark, E.G. Jones and J. Yan, Numbers and proportions of GABA-immunoreactive neurons in different areas of monkey cerebral cortex, J. Neurosci. **7**, 1503-1519 (1987).

[37] J.L. Rubenstein and M.M. Merzenich, Model of autism: increased ratio of excitation/inhibition in key neural systems, Genes Brain Behav. **2**, 255-67 (2003).

[38] P. Levitt, K.L. Eagleson and E.M. Powell, Regulation of neocortical interneuron development and the implications for neurodevelopmental disorders, Trends Neurosci. **27**, 400-6 (2004).

[39] O. Yizhar, L.E. Fenno, M. Prigge, F. Schneider, T.J. Davidson, D.J. O'Shea et al., Neocortical excitation/inhibition balance in information processing and social dysfunction, Nature **477**, 171-178 (2011).

[40] D.A. Lewis, K.N. Fish, D. Arion and G. Gonzalez-Burgos, Perisomatic inhibition and cortical circuit dysfunction in schizophrenia, Curr. Opin. Neurobiol. **21**, 866-72 (2011).

[41] O. Marin, Interneuron dysfunction in psychiatric disorders. Nat. Rev. Neurosci. **13**, 107-20 (2012).

[42] V. Latora and M. Marchori, Efficient Behavior of Small-World Networks, Phys. Rev. Lett. **87**, 198701 (2001).

[43] G. Buzsaki and K. Mizuseki, The log-dynamic brain: how skewed distributions affect network operations, Nat. Neurosci. **15**, 264-278 (2014).

[44] E.S.C. Ching and P.H. Tam, Effects of hidden nodes on the reconstruction of bidirectional networks, Phys. Rev. E **98**, 062318 (2018).

[45] When $|f_{ij}(\tau)|$ attains its maximum at more than one value of τ, all of the same sign, τ^* is taken as the τ-value with the minimum magnitude. If the values of τ at which $|f_{ij}(\tau)|$ attains its maximum include both positive and negative values, then we take τ^* as the τ-value with the minimum magnitude separately for the positive and negative τ-values. If these two τ^* both satisfy the criterion set by the maximum propagation speed of synaptic signal, then there are bidirectional links between nodes i and j with the same coupling strength in either direction.

[46] A.X.C.N. Valente, A. Sarkar, H.A. Stone, Two-peak and three-peak optimal complex networks, Phys. Rev. Lett. **92**, 118702 (2004).

[47] T. Tanizawa, G. Paul, R. Cohen, S. Havlin and H.E. Stanley, Optimization of network robustness to waves of targeted and random attacks, Phys. Rev. E **71**, 047101 (2005).